Density Functional Theory Study of Decarboxylation and Decarbonylation of Acetic Acid on Pd (111)

*Kingsley C. Chukwu and Líney Árnadóttir**

School of Chemical, Biological and Environmental Engineering, Oregon State University, Corvallis, OR, 97331, United States.

ABSTRACT

Acetic acid (CH_3COOH) decomposition over Pd (111) surface is a good model system for decomposition of acids and small oxygenates common in biomass conversion. Here we present Density Functional Theory calculations of the energy landscape of CH_3COOH decomposition on Pd (111), focusing on the reaction mechanism for acetic acid decarboxylation (DCX) and decarbonylation (DCN). Our results suggest that the most favorable DCX pathway proceeds through dehydrogenation of CH_3COOH to acetate (CH_3COO), followed by dehydrogenation of CH_3COO to carboxylmethylidene (CH_2COO), C-H bond cleavage of CH_2COO to carboxylmethylidyne (CHCOO) and finally C-C bond cleavage to form CH and CO_2. The DCN pathway proceeds via the same initial dehydrogenation steps to CH_2COO, followed by deoxygenation of the CH_2COO to ketene (CH_2CO). This follows dehydrogenation of CH_2CO to

ketyne (CHCO), and finally C-C bond cleavage to yield CH and CO. Carboxylmethylidene (CH_2COO), which is formed in both mechanism, is a key reaction intermediate determining the branching to DCN or DCX but the free energy barrier difference between the DCN and the DCX route is $\Delta G_a = 0.13$eV, making the DCX more favorable than DCN.

1. INTRODUCTION

The decomposition of acetic acid on the Pd (111) surface is of both fundamental and applied interest. The interaction of acetic acid with Pd (111) is key to the production of vinyl acetate (a precursor to important industrial polymer such as polyvinyl acetate), biomass conversion to biofuels, and other industrial relevant reactions.[1-3] Acetic acid is also a good model for selectivity studies of long fatty acid on Pd and Pt, which are among the major catalyst metals used in the production of bio-fuels.[3]

In this study, we focused on the reaction mechanism of acetic acid decarboxylation (DCX) and decarbonylation (DCN) on Pd (111) but acetic acid decarboxylation and decarbonylation have been found to reduce the selectivity of acetic acid conversion to vinyl acetate on Pd (111).[2] Experimental studies of acetic acid decomposition on Pd (111) and Pd (100) catalyst in ultrahigh vacuum yielded CO, CO_2, H_2O, and H_2,[4-6] while over Pd (110), acetic acid decomposes to CO_2 and H_2, in which the H_2 is converted to H_2O in the presence of pre-adsorbed oxygen during acetic decomposition.[7] The decarboxylation route, producing CO_2, was found to be the preferred route on Pd(111) and the rate determining step was the activation of the C-H bond of the methyl group of the surface acetate.[6] These observations suggest that OC-O and C-OH bond cleavages of acetic

acid intermediates are less facile on Pd (110) and OC-O and C-OH bond cleavages are important elementary reaction steps in the formation of CO and H_2O during acetic acid decomposition.

Understanding the reaction mechanism of acetic acid decomposition on Pd (111) could also provide insight into other reaction pathways with similar intermediates such as hydrogenation of acetic acid to ethanol, which has been studied both experimentally and by different theoretical approaches on various transition metals and supported transition metals.[8-14]

Here we present a DFT study of acetic acid decomposition on Pd (111) surface, in which all the elementary reaction steps involved in acetic acid decomposition to H_2O, H_2, CO_2 and CO were investigated and the preferred reaction mechanisms for acetic acid decarboxylation and decarbonylation were proposed. Hansen and Neurock[1] studied acetic acid decomposition on Pd (111) previously using DFT calculated reaction energies and stochastic kinetic algorithms. This study focused on modeling the trends observed in experimental temperature-programmed reaction experiments (TPR) for acetic acid decomposition over Pd (111) and included subset of elementary steps studied herein, specifically that study included elementary steps 2, 5, 16, 38, 39, 44, 45, and 46 from Table 2. Previous experimental studies have shown that full decomposition of acetic acid on Pd (111) produces CO, CO_2 and surface C via either decarbonylation or decarboxylation pathways.[4] Here we focus on the interplay between these two decomposition pathways on Pd (111). In order to compare these different pathways, all elementary steps, except C=O cleavage, leading to the formation of CO and CO_2 are included. The elementary steps involving C=O bond cleavage, for intermediates CH_xCO; x=0-3 and CH_yCOOH; y=0-3, were not included because they were previously found to have significantly higher activation barrier and reaction energy than C-O, C-C and C-H bond scission.[9, 15] The decomposition of CH_x to surface carbon is the same for both pathways and therefore not included in the discussion of the two pathways. The energetic of

CH_x dissociation are included in Table 2 and an energy diagram for the dissociation is in the supporting information.

2. METHODS

Density functional theory calculations were carried out using the Vienna Ab initio Simulation Package (VASP).[16-19] The Kohn-Sham equations were solved with a plane-wave basis set and core electrons were described using the projector augmented wave (PAW) method.[20] Electron exchange and correlation were described within the PW91 generalized gradient approximation (GGA).[21-23] Spin polarization was used for all calculations, and the cutoff energy for the plane wave basis set was 400 eV.

The calculated Pd lattice constant was 3.96 Å, in good agreement with experimental results of 3.89 Å.[24] The Pd (111) surface was represented by a four-atomic layer slab using a (3×4) unit cell, corresponding to surface coverage (θ) of 1/12 monolayer (ML) for each adsorbate (where ML is defined as number of adsorbates/metal surface atom), which is in good agreement with acetic acid coverage (0.1ML) in experimental studies of acetic acid decomposition on Pd (111).[6] All adsorbates and the two topmost Pd layers were allowed to relax, the remaining layers were kept fixed. A total vacuum distance of 17 Å was used to separate the surface from its periodic slab in the direction along the surface normal. Zero-point energy (ZPE) is not included in reaction energies and activation barriers reported herein. A Monkhorst–Pack grid of 4 × 4 × 1 k-points was used for all calculations.

Adsorption energies (E_{ads}) of all the surface intermediates were calculated as

$$E_{ads} = E_{s+ads} - E_s - E_{ref}$$

where E_{s+ads} is the total energy of the slab with the adsorbate, E_s is the total energy of the clean Pd slab and E_{ref} is the total energy of the adsorbate in their most stable configuration in the gas phase, used as reference. The reaction energies (E_{rxn}) for a reaction of the form A+B⟶AB is the energy difference between the reactants (E_{S+A+B}) and the products (E_{S+AB}) ($E_{rxn} = E_{s+A+B} - E_{s+AB}$).

In this notation, more negative adsorption energies equate to more favorable adsorbate configuration and negative reaction energies equate to exothermic reactions while positive reaction energies equate to endothermic reactions. The minimum energy path from reactant to product and the transition state for each elementary reaction step were calculated with the climbing image nudged elastic band (Cl-NEB)[25-28] method. All transition states were confirmed by vibrational analysis to have only one imaginary frequency, these imaginary frequencies are listed in Table S1 in supporting information. The convergence criteria for the maximum residual force for the adsorbate binding and CI-NEB calculations were 0.03 and 0.05 eV/Å, respectively. Standard statistical mechanics approach was used to the Gibbs free reaction and activation energies at 300K.[29]

3. RESULTS

The elementary reaction steps investigated for decarboxylation (DCX) reaction pathways to CO_2 and decarbonylation (DCN) reaction pathways to CO of acetic acid decomposition on Pd (111) are shown in Figure 1. All reaction intermediates and activation barriers of all elementary reaction steps included in this study are described in sections 3.1 and 3.2.

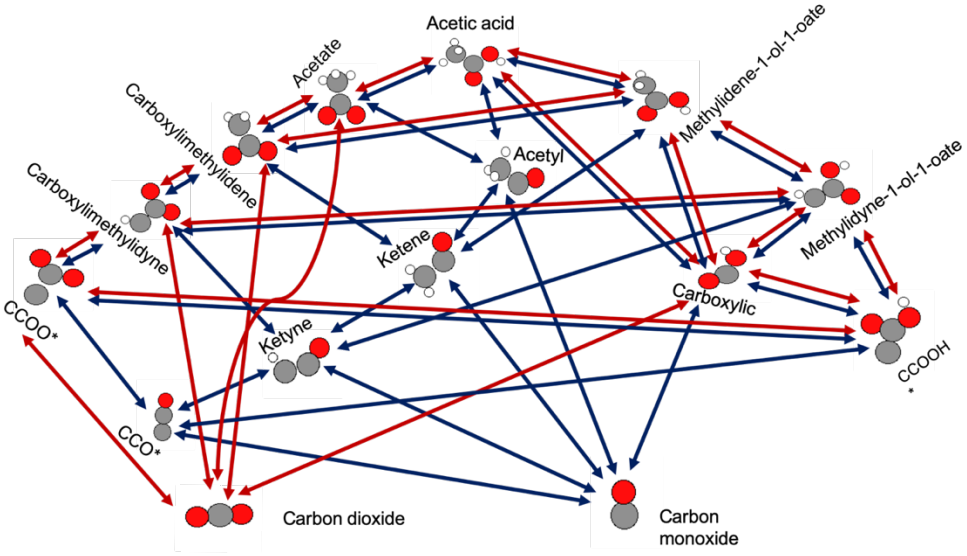

Figure 1. Reaction network of the decarboxylation (red arrows) and decarbonylation (blue arrows) pathways of acetic acid decomposition on Pd (111). Two arrows indicate that the decarboxylation and decarbonylation pathways go through the same elementary reaction step.

3.1. Reaction intermediates

The most stable adsorption configurations of all reactants, products and intermediates of acetic acid decomposition on Pd (111) are shown in Figure 2. The most stable binding modes and adsorption energies of the different intermediates are listed in Table 1, in agreement with previous literature.[1,9,15,30-33] Phatak et al.[32] identified two isoenergic adsorption configurations for OH, which are linear OH on fcc site and a tilted OH on the bridge site. The latter was found to be the most favorable adsorption configuration herein.

We use the nomenclature ηiμj to represent i atoms of the adsorbates bound to j atoms of the metal surface. To clearly distinguish the different carbon atoms in this discussion, the carbon in the COOH functional group is referred to as C_1 and the α-carbon as C_2. Apart from CH_3COOH, CO_2 and H_2O, ketene has the weakest binding to Pd (111) of all reaction intermediates and carbon

atom have the strongest binding, in good agreement with experimentally reported coke formation on Pd (111) surfaces.[4]

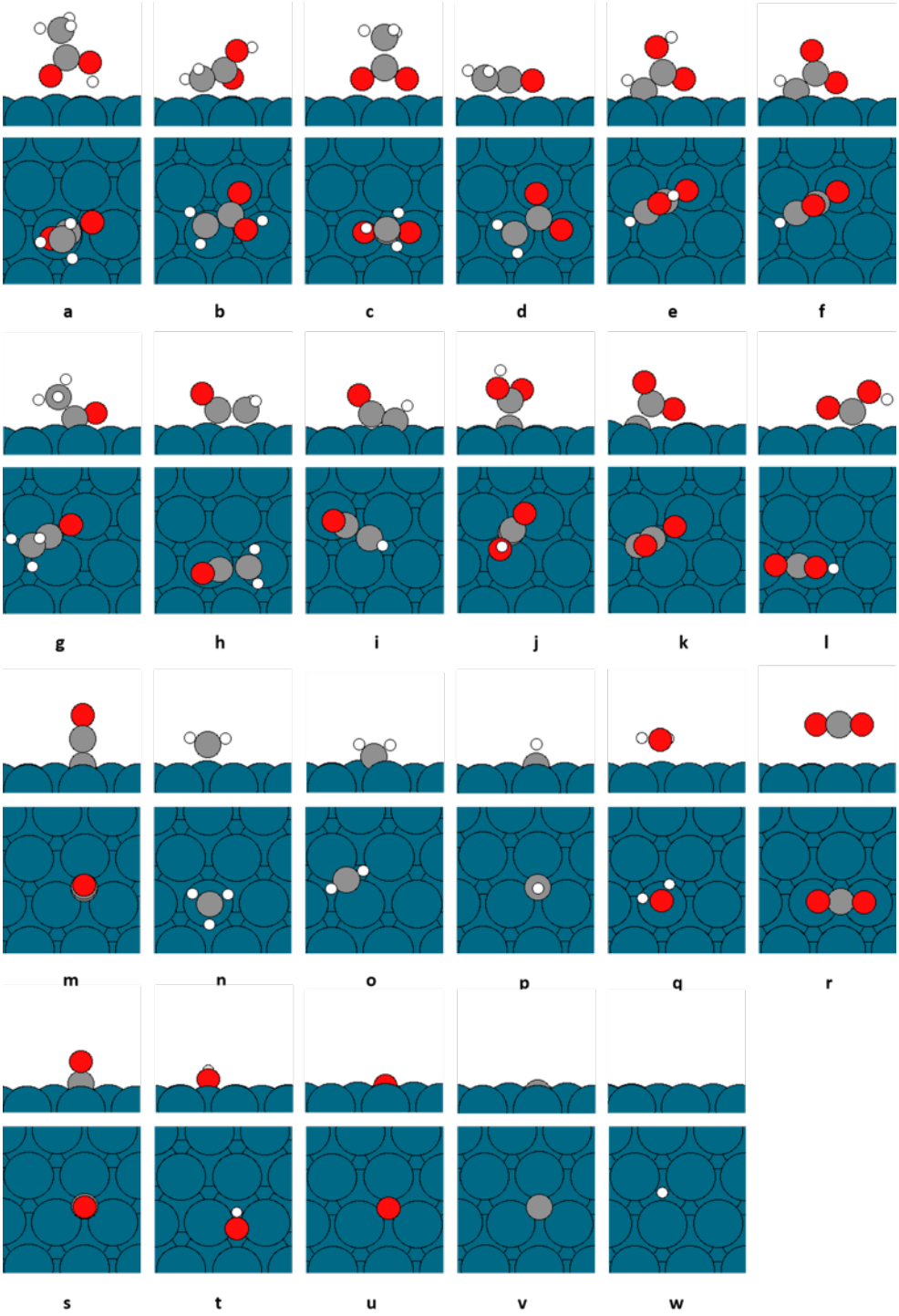

Figure 2. Side and top views of the most stable adsorption configurations of the reaction intermediates in acetic acid decomposition on Pd (111): (a) acetic acid (CH_3COOH); (b) methylidene-1-ol-1-olate (CH_2COOH); (c) acetate (CH_3COO); (d) carboxylmethylidene (CH_2COO); (e) methylidyne-1-ol-1-olate (CHCOOH); (f) carboxylmethylidyne (CHCOO); (g) acetyl (CH_3CO); (h) ketene (CH_2CO); (i) ketyne (CHCO); (j) CCOOH; (k) CCOO; (l) carboxylic (COOH); (m) CCO; (n) methyl (CH_3); (o) methene (CH_2); (p) methyne (CH); (q) water (H_2O); (r) carbon dioxide (CO_2); (s) carbon monoxide (CO); (t) hydroxyl (OH); (u) oxygen (O); (v) carbon (C); and (w) hydrogen (H). Pd surface atoms are shown in blue, oxygen in red, hydrogen in white and carbon in gray.

Table 1. Binding modes, binding sites, and adsorption energies of all adsorbed intermediates investigated. In the $\eta i\mu j$ binding mode nomenclature *i* atoms of the adsorbates are bound to *j* atoms of the metal surface. The adsorbate atom C_1 represents the carbon in the COOH functional group and C_2 represents the α-carbon. The adsorption energies do not include for zero-pointed energy correction.

Species	Stoichiometry	Figure 3 Species	Binding mode	Binding site	Adsorption energy (eV)
Acetic acid	CH_3COOH	a	$\eta 1\mu 1$(O)	O(atop)	-0.48
Methylidene-1-ol-1-olate	CH_2COOH	b	$\eta 2\mu 2$(C, O)	C_2(atop), O(atop)	-2.07
Acetate	CH_3COO	c	$\eta 2\mu 2$(O, O)	O(atop), O(atop)	-2.34
Carboxylmethylidene	CH_2COO	d	$\eta 3\mu 3$(C, O, O)	C_2(atop), O(atop), O(atop)	-1.49

Methylidyne-1-ol-1-olate	CHCOOH	e	$\eta 2\mu 3$(C, O)	C_2(bridge), O(atop)	-4.00
Carboxylmethylidyne	CHCOO	f	$\eta 2\mu 3$(C, O)	C_2(bridge), O(atop)	-2.04
Acetyl	CH_3CO	g	$\eta 2\mu 3$(C, O)	C_1(bridge), O(atop)	-2.22
Ketene	CH_2CO	h	$\eta 2\mu 2$(C, C)	C_1(atop), C_2(atop)	-1.16
Ketyne	CHCO	i	$\eta 2\mu 3$(C, C)	C_1(atop), C_2(bridge)	-3.17
	CCOOH	j	$\eta 1\mu 3$(C)	C_2(fcc hollow)	-5.41
	CCOO	k	$\eta 2\mu 4$(C, O)	C_1(hcp hollow), O(atop)	-4.11
Carboxylic	COOH	l	$\eta 2\mu 2$(C, O)	C_1(atop), O(atop)	-2.38
	CCO	m	$\eta 1\mu 3$(C)	C_2(fcc hollow)	-5.01
Methyl	CH_3	n	$\eta 1\mu 1$(C)	C_2(atop)	-1.90
Methene	CH_2	o	$\eta 1\mu 2$(C)	C_2(bridge)	-4.02
Methyne	CH	p	$\eta 1\mu 3$(C)	C_2(hollow)	-6.54
Water	H_2O	q	$\eta 1\mu 1$(O)	O(atop)	-0.32
Carbon dioxide	CO_2	r	$\eta 2\mu 2$(O, O)	O(atop), O(atop)	-0.09
Carbon monoxide	CO	s	$\eta 1\mu 3$(C)	C_1(fcc hollow)	-2.05
Hydroxyl (bent)	OH	t	$\eta 1\mu 2$(O)	O(bridge)	-2.71
Oxygen atom	O	u	$\eta 1\mu 3$(O)	O (fcc hollow)	-1.43
Carbon atom	C	v	$\eta 1\mu 3$(C)	C (fcc hollow)	-7.06
Hydrogen atom	H	w	$\eta 1\mu 3$(H)	H (hcp hollow)	-2.88

The dehydrogenation of the α-carbon of CH_XCOOH (x =1, 2, 3) decreases the adsorption energy of the product, similar to what was previously reported for dehydrogenation products of propanoic acid intermediates on Pd(111).[31] Dehydrogenation of the α-carbon of CH_xCO (x =1, 2) also decreases the adsorption energy of the products but dehydrogenation of CH_3CO to CH_2CO increases the adsorption energy. Li et al.[15] found a similar trend for dehydrogenation of CH_3CO to CH_2CO on Pd (111) as well as Lu et al.[29] for dehydrogenation of CH_3CH_2CO to CH_3CHCO on Pd (111). Dehydrogenation of the α-carbon of CH_X (x = 1, 2, 3) decreases the adsorption energy of the product, similar to the trend reported by Li et al.[14]

3.2 Elementary reaction steps for acetic acid decomposition over Pd (111)

The activation barriers and reaction energies for each elementary reaction step of the different reaction pathways are summarized in Table 2. For more complex minima energy pathways, an intermediate adsorption configuration was sometimes used to determine the activation barriers, these are noted in the description of the reaction step. These intermediate adsorption configurations were determined from the initial CI-NEB calculations. The configurations of the different transition states are shown in Figure 3 and Figure 4 while intermediate adsorption configurations used for Cl-NEB calculations for elementary reaction steps 2, 3, 6 and 15 are shown in Figure 5. These intermediate adsorption configurations were used to activate the various bonds involved in the bond cleavage during the different reaction steps. The reaction energies and activations barriers for the transition from the minima to these intermediate configurations are noted in the description of each individual elementary steps. All reaction energies and barriers heights are referenced to the most stable adsorbate configuration.

In general, dehydrogenation of the α-carbon of CH_XCOOH (x = 2, 3) increases the activation barrier for the dehydrogenation of the CO-H bond of CH_XCOOH (x = 1, 2). Dehydrogenation of the α-carbon of CH_XCO (x = 2, 3) and CH_xCOO (x = 1, 2, 3) reduces the activation barrier for the C-C bond cleavage of CH_xCO (x = 1, 2) and CH_xCOO (x = 0, 1, 2, 3). These are in good agreement with previous calculations of CO-H bond and C-C bond cleavage on Pd(111).[15, 31] The elementary reaction steps for C=O bond scission in these intermediate (CH_xCO; x=0-3) and (CH_xCOOH; x=0-3) were not included because they were previously found to have significantly higher activation barriers and reaction energies than C-O, C-C and C-H bond scission.[9, 15]

Table 2. Reaction energies and forward activation barriers for decomposition of acetic acid on Pd (111). The * indicates adsorbed molecule and available adsorption site and not the number of sites available or occupied by the adsorbates. The reaction energies and forward activation barrier were not corrected for zero-point energy.

steps	surface reactions	E_{rxn}[eV]	E_a[eV]
1	$CH_3COOH^* + * \rightarrow CH_3^* + COOH^*$	0.66	1.91
2	$CH_3COOH^* + * \rightarrow CH_3COO^* + H^*$	-0.07	0.69
3	$CH_3COOH^* + * \rightarrow CH_3CO^* + OH^*$	0.83	1.23
4	$CH_3COOH^* + * \rightarrow CH_2COOH^* + H^*$	0.30	1.06
5	$CH_3COO^* + * \rightarrow CH_2COO^* + H^*$	0.79	1.37
6	$CH_3COO^* + * \rightarrow CH_3^* + CO_2^*$	0.36	1.92
7	$CH_3COO^* + * \rightarrow CH_3CO^* + O^*$	1.02	1.56
8	$CH_2COOH^* + * \rightarrow COOH^* + CH_2^*$	0.44	1.33
9	$CH_2COOH^* + * \rightarrow CH_2CO^* + OH^*$	0.71	1.19
10	$CH_2COOH^* + * \rightarrow CHCOOH^* + H^*$	0.13	0.91
11	$CH_2COOH^* + * \rightarrow CH_2COO^* + H^*$	0.45	1.33

12	$CHCOOH^* + * \rightarrow CHCO^* + OH^*$	0.73	1.68
13	$CHCOOH^* + * \rightarrow CCOOH^* + H^*$	-0.20	0.64
14	$CHCOOH^* + * \rightarrow COOH^* + CH^*$	-0.09	1.00
15	$CHCOOH^* + * \rightarrow CHCOO^* + H^*$	0.51	1.57
16	$CH_2COO^* + * \rightarrow CH_2^* + CO_2^*$	-0.27	1.36
17	$CH_2COO^* + * \rightarrow CH_2CO^* + O^*$	0.36	0.98
18	$CH_2COO^* + * \rightarrow CHCOO^* + H^*$	0.17	0.94
19	$CHCOO^* + * \rightarrow CCOO^* + H^*$	-0.08	0.79
20	$CHCOO^* + * \rightarrow CH^* + CO_2^*$	-0.90	0.61
21	$CHCOO^* + * \rightarrow CHCO^* + O^*$	0.20	1.21
22	$CH_3CO^* + * \rightarrow CH_2CO^* + H^*$	0.29	1.08
23	$CH_3CO^* + * \rightarrow CH_3^* + CO^*$	-0.51	1.11
24	$CH_2CO^* + * \rightarrow CH_2^* + CO^*$	-0.65	1.02
25	$CH_2CO^* + * \rightarrow CHCO^* + H^*$	-0.14	0.83
26	$CHCO^* + * \rightarrow CH^* + CO^*$	-1.04	0.51
27	$CHCO^* + * \rightarrow CCO^* + H^*$	-0.06	1.07
28	$CCOOH^* + * \rightarrow COOH^* + C^*$	0.51	1.78
29	$CCOOH^* + * \rightarrow CCOO^* + H^*$	0.63	1.25
30	$CCOOH^* + * \rightarrow CCO^* + OH^*$	0.99	1.42
31	$COOH^* + * \rightarrow CO^* + OH^*$	-0.31	0.66
32	$COOH^* + * \rightarrow CO_2^* + H^*$	-0.29	0.74
33	$CCOO^* + * \rightarrow CO_2^* + C^*$	-0.46	0.31
34	$CCOO^* + * \rightarrow CCO^* + O^*$	0.44	1.03
35	$CCO^* + * \rightarrow CO^* + C^*$	-0.36	0.90
36	$CH_3^* + * \rightarrow CH_2^* + H^*$	0.16	0.87
37	$CH_2^* + * \rightarrow CH^* + H^*$	-0.56	0.33
38	$CH^* + * \rightarrow C^* + H^*$	0.45	1.44
39	$OH^* + H^* \rightarrow H_2O^* + *$	-0.41	0.69

40	$CO^* + O^* \rightarrow CO_2^* + *$	0.02	1.63
41	$C^* + O^* \rightarrow CO^* + *$	-2.67	1.25
42	$OH^* + * \rightarrow O^* + H^*$	0.07	1.06
43	$H^* + H^* \rightarrow H_{2(g)} + 2^*$	1.20	
44	$CO^* \rightarrow CO_{(g)} + *$	2.05	
45	$CO_2^* \rightarrow CO_{2(g)} + *$	0.09	
46	$H_2O^* \rightarrow H_2O_{(g)} + *$	0.32	

Step 1: $CH_3COOH \longrightarrow CH_3 + COOH$. The overall endothermicity of this reaction is 0.66eV and it has a relatively high activation barrier of 1.91eV. Similar high activation barrier (3.53eV) was observed for the C-C bond cleavage of ethanol.[15] In the transition state (TS), both CH_3 and COOH sit above a top site and the C-C bond length changes from 1.49Å (initial state (I.S) bond length) to 2.02Å.

Step 2: $CH_3COOH \longrightarrow CH_3COO + H$. Before the O-H dissociation, the CH_3COOH rotates to a configuration whereby the COOH group has both the O and H above a top site (see Figure 5(i) for this adsorption configuration). This configuration is 0.08eV higher in energy than the minima configuration and the rotation have no barrier. The reaction is exothermic by 0.07eV and has an activation barrier of 0.69eV, in reasonable agreement with Hansen and Neurock,[1] who reported a 0.55eV activation barrier for this reaction. The transition state (TS) is characterized by O-H bond elongation from 1.02Å (I.S bond length) to 1.62Å, in which the H is over a bridge site.

Step 3: $CH_3COOH \longrightarrow CH_3CO + OH$. In order to activate the C-OH bond, the acetic acid rotates from the most favorable configuration to a less favorable configuration in which the two oxygen atoms interact with the surface (see Figure 5(ii) for this adsorption configuration). This adsorption configuration is 0.08eV higher in energy than the minima and the rotation have no barrier. This reaction is endothermic by 0.83eV and has an activation barrier of 1.23eV, in reasonable agreement

with Pallassana and Neurock,[9] who reported an activation barrier of 1.47eV for the same step. The TS is characterized by a C-OH bond elongation from 1.33Å (I.S bond length) to 2.07Å, in which the OH is above a top site.

Step 4: $CH_3COOH \longrightarrow CH_2COOH + H$. The α-carbon dehydrogenation of CH_3COOH is endothermic by 0.30eV and has an activation barrier of 1.06eV, in reasonable agreement with the activation barrier for α-carbon dehydrogenation of ethanol (E_a=1.17eV).[15] The TS is characterized by a C-H bond elongation from 1.1Å (I.S bond length) to 1.59Å, in which the H is above a bridge site.

Step 5: $CH_3COO \longrightarrow CH_2COO + H$. In this reaction step, the CH_3COO reorients from a bidentate to tridentate adsorption mode (see Figure 5(iii) for this adsorption configuration) before activating the C-H bond cleavage. This reaction is endothermic by 0.79eV and has a comparatively high activation barrier of 1.37eV. Pallassana and Neurock[9] previously reported an activation barrier and reaction energy for this reaction to be 1.19eV and 0.72eV, respectively. In the TS, the H is above a bridge site and the C-H bond distance changes from 1.09Å (I.S bond length) to 1.57Å.

Step 6: $CH_3COO \longrightarrow CO_2 + CH_3$. The decarboxylation of the CH_3COO follows two successive steps. A reorientation from bidentate to tridentate configurations, in which the CH_3COO is lying down. This reorientation has a reaction energy of 0.70eV and no barrier. The C-C bond cleavage occurs after the reorientation. The overall endothermicity of the two-step reaction is 0.36eV and the activation barrier is 1.92eV based on the most stable initial state, but 1.22 eV from the intermediate state. At the TS, the CH_3 sits above a top site and the C-C bond distance changes from 1.51Å (I.S bond length) to 2.02Å.

Step 7: $CH_3COO \longrightarrow CH_3CO + O$. In the initial state, the bidentate CH_3COO adsorbs with each oxygen atom on a top site. Before C-O bond scission, the CH_3COO rotates so that one of the

oxygen atoms is above a bridge site. The deoxygenation of CH_3COO to CH_3CO is endothermic by 1.02eV and has a relatively high activation barrier of 1.56eV. The TS is characterized by a C-O bond elongation from 1.30Å (I.S bond length) to 1.97Å, in which the O sits above a hollow site and the α-carbon is above a top site.

Step 8: $CH_2COOH \longrightarrow CH_2 + COOH$. The H_2C-COOH bond cleavage of CH_2COOH has an activation barrier of 1.33eV and is endothermic by 0.44eV. The TS is characterized by a H_2C-COOH bond elongation from 1.46Å (I.S bond length) to 2.29Å, in which the CH_2 group is above a bridge site and the COOH group is above a top site.

Step 9: $CH_2COOH \longrightarrow CH_2CO + OH$. Dehydroxylation of CH_2COOH is endothermic by 0.71eV and has an activation barrier of 1.19eV. The TS is described by a C-OH bond elongation from 1.35Å (I.S bond length) to 2.14Å, in which both OH and CH_2CO are above a top site.

Step 10: $CH_2COOH \longrightarrow CHCOOH + H$. The dehydrogenation of CH_2COOH to CHCOOH is endothermic by 0.13eV and has an activation barrier of 0.91eV. In the TS, the C-H bond length changes from 1.10Å (I.S bond length) to 1.72Å and the α-carbon sits above the bridge site while the H sits above a top site.

Step 11: $CH_2COOH \longrightarrow CH_2COO + H$. The dehydrogenation of CH_2COOH is endothermic by 0.45eV and its activation barrier is 1.33eV. In the TS, the activated H sits above a top site and the O-H bond length elongates from 0.98Å (I.S bond length) to 1.76Å.

Step 12: $CHCOOH \longrightarrow CHCO + OH$. Similar to step 5, the CHCOOH reorients from a bidentate to a tridentate form, so as to activate the C-OH bond. This reorientation has a reaction energy of 0.47eV and no barrier. This reaction step is endothermic by 0.73eV and has a relatively high activation barrier, 1.68eV. The TS is characterized by the C-OH bond elongation from 1.35Å (I.S bond length) to 2.02Å, in which the OH sits above a top site.

Step 13: CHCOOH⟶H + CCOOH. The CHCOOH reorients from a bidentate to a monodentate form before C-H bond cleavage. The reaction is exothermic by 0.20eV and its activation barrier is 0.64eV. In the TS, the H sits above a hollow site and the C-H bond length elongates from 1.10Å (I.S bond length) to 1.36Å.

Step 14: CHCOOH⟶CH + COOH. The HC-COOH bond scission of CHCOOH has an activation barrier of 1.00eV and reaction energy of -0.09eV. The TS is characterized by a C-COOH bond length elongation from 1.46Å (I.S bond length) to 1.92Å, in which the CH group sits above a hollow site.

Step 15: CHCOOH⟶CHCOO + H. For the dehydrogenation of CHCOOH, the reaction follows two successive steps. A CHCOOH reorientation from a bidentate to tridentate configuration, in which the oxygen of the OH group sits above a top site (see Figure 5(iv) for this adsorption configuration). This reorientation has a reaction energy of 0.47eV and no barrier. The CO-H bond cleavage occurs after the reorientation. The overall reaction energy of the two steps is 0.51eV and the activation barrier is 1.57eV based on the most stable initial state, but 1.10 eV from the intermediate state. The TS is characterized by an O-H bond distance increase from 0.98Å (I.S bond length) to 1.61Å, in which the H sits above a top site.

Step 16: $CH_2COO \longrightarrow CH_2 + CO_2$. This reaction is exothermic by 0.27eV and the activation energy is 1.36eV. At the TS, the C-C bond distance elongates from 1.47Å (I.S bond length) to 2.14Å and CH_2 sits above a top site.

Step 17: $CH_2COO \longrightarrow CH_2CO + O$. The deoxygenation of CH_2COO is endothermic by 0.36eV and the reaction has an activation barrier of 0.98eV. The TS is characterized by a C-O bond distance that extends from 1.30Å (I.S bond length) to 1.99Å, in which the O sits above a fcc hollow site.

Step 18: $CH_2COO \rightarrow CHCOO + H$. The CH_2COO reorients from a tridentate to a bidentate configuration before C-H bond cleavage. The reaction is endothermic by 0.17eV and the activation energy is 0.94eV. In the TS, the C-H bond length elongates from 1.10Å (I.S bond length) to 1.71Å and the α-carbon sits above a bridge site, while the activated H sits above a top site.

Step 19: $CHCOO \rightarrow CCOO + H$. The dehydrogenation of CHCOO to CCOO is slightly exothermic with a reaction energy of -0.08eV and an activation barrier of 0.79eV. The TS is characterized by C-H bond elongation from 1.10Å (I.S bond length) to 1.46Å, in which the H sits above a bridge site.

Step 20: $CHCOO \rightarrow CH + CO_2$. The decarboxylation of CHCOO is quite exothermic by 0.90eV and has an activation barrier of 0.61eV. In the TS, the C-C bond length elongates from 1.50 Å (I.S bond length) to 1.96Å. In the final state, the CO_2 is adsorbed on a top site and CH is adsorbed on the fcc hollow site.

Step 21: $CHCOO \rightarrow CHCO + O$. The deoxygenation of CHCOO to CHCO is endothermic by 0.20eV and has an activation barrier of 1.21eV. In the TS, the O is above a bridge site and the C-O bond length elongates from 1.23Å (I.S bond length) to 1.97Å.

Step 22: $CH_3CO \rightarrow CH_2CO + H$. This reaction is endothermic by 0.29eV and the activation barrier is 1.08eV. The TS is characterized by a C-H bond elongation from 1.10Å (I.S bond length) to 1.55Å, in which the H sits above a bridge site.

Step 23: $CH_3CO \rightarrow CH_3 + CO$. This reaction is exothermic by 0.51eV and the activation barrier is 1.11eV. In the TS, the C-C bond length extends from 1.58Å (I.S bond length) to 1.93Å.

Step 24: $CH_2CO \rightarrow CH_2 + CO$. The α-carbon of CH_2CO reorients from a top site to sit above a bridge site before C-C bond cleavage. This reorientation has no barrier and its reaction energy is

0.29eV. This elementary reaction step is exothermic by 0.65eV and the activation barrier is 1.02eV. Between the initial and the TS, the C-C bond length increases from 1.48Å to 2.01Å.

Step 25: $CH_2CO \rightarrow CHCO + H$. The dehydrogenation of CH_2CO to CHCO is exothermic by 0.14eV and has an activation barrier of 0.83eV. The TS is characterized by a C-H bond length that extends from 1.10Å to 1.70Å going from the initial to the TS. At the TS, the α-carbon is over a bridge site and the H is over a top site.

Step 26: $CHCO \rightarrow CH + CO$. The decarbonylation of CHCO is exothermic by 1.04eV and has an activation barrier of 0.51eV. The TS is characterized by an increase of C-C bond length from 1.43Å (I.S bond length) to 1.91Å. In the TS, the CO sits above a top site and CH sits above a hollow site.

Step 27: $CHCO \rightarrow CCO + H$. The dehydrogenation of CHCO is close to thermoneutral with a reaction energy of -0.06eV and an activation barrier of 1.07eV, in reasonable agreement with previous findings from Li et al.[15] In the TS, the H sits above a top site and the C-H bond elongates from 1.01Å to 1.69Å relative to the initial state.

Step 28: $CCOOH \rightarrow C + COOH$. The C-COOH bond scission of CCOOH is endothermic by 0.51eV and has an activation barrier of 1.78eV. In the TS, the COOH sits above a top site and the C-COOH bond length is 0.52 Å longer than that of the initial state.

Step 29: $CCOOH \rightarrow CCOO + H$. The CCOOH dehydrogenation is endothermic by 0.63eV and its activation barrier is 1.25eV. In the TS, the H is above the bridge site and the O-H bond length extends from 0.98Å to 1.81Å relative to the initial state.

Step 30: $CCOOH \rightarrow CCO + OH$. The dehydroxylation of CCOOH to CCO is endothermic by 0.99eV and has an activation energy of 1.42eV. The TS is characterized by the C-OH bond elongation from 1.37Å (I.S bond length) to 2.46Å, in which the OH is above a top site.

Step 31: COOH⟶CO + OH. The dehydroxylation of COOH is exothermic by 0.31eV and has an activation barrier of 0.66eV. The TS is characterized by an increase of the C-OH bond length from 1.34Å (I.S bond length) to 1.88Å, in which the OH sits above a top site and the CO sits above a bridge site.

Step 32: COOH⟶CO_2 + H. The decarboxylation of the COOH is exothermic by 0.29eV and the reaction has an activation barrier of 0.74eV, in good agreement with finding from Scaranto and Mavrikakis,[34] who calculated the activation barrier for this reaction to be 0.70eV. The TS is characterized by O-H bond elongation from 0.98Å (I.S bond length) to 1.51Å, in which the hydrogen atom sits above a top site.

Step 33: CCOO⟶CO_2 + C. Decarboxylation of CCOO is exothermic by 0.46eV and has low activation barrier of 0.31eV. The TS is characterized by C-C bond elongation from 1.53Å (I.S bond length) to 1.95Å.

Step 34: CCOO⟶CCO + O. The deoxygenation of CCOO is endothermic by 0.44eV and has an activation barrier of 1.03eV. The TS is characterized by a C-O bond elongation from 1.31Å (I.S bond length) to 2.05Å.

Step 35: CCO⟶CO + C. The decarbonylation of CCO is exothermic by 0.36eV and its activation barrier is 0.90eV. The TS is characterized by C-CO bond elongation from 1.34Å (I.S bond length) to 1.87Å, in which the CO molecule sits above a bridge site.

Step 36: CH_3⟶CH_2 + H. CH_3 moves from a top site to a bridge site before C-H bond cleavage. The reaction is endothermic by 0.16eV and has an activation barrier of 0.87eV. The TS is characterized by a C-H bond distance elongation from 1.09Å (I.S bond length) to 1.76Å, in which the C sits above the bridge site and H sits above a top site.

Step 37: $CH_2 \longrightarrow CH + H$. Dehydrogenation of CH_2 is exothermic by 0.56eV and has a relatively low activation barrier of 0.33eV. In the TS, both the CH and H sit on a hollow site and the C-H bond distance extends from 1.10Å (I.S bond length) to 1.94Å.

Step 38: $CH \longrightarrow C + H$. Dissociation of CH is endothermic by 0.45eV and its activation barrier is 1.44eV. The TS is characterized by a C-H bond length elongation from 1.10Å (I.S bond length) to 1.76Å, in which the H sits on a top site and C sits on a hollow site.

Step 39: $OH + H \longrightarrow H_2O$. Formation of water on the surface is exothermic by 0.41eV and has a relatively low activation barrier of 0.69eV, in good agreement with findings of Scaranto and Mavrikakis.[34] The TS is characterized by a H-OH bond extension from 0.98Å (I.S bond length) to 1.64Å, in which the OH and H sit on the top site and bridge site respectively.

Step 40: $CO + O \longrightarrow CO_2$. The oxygenation of CO is almost thermoneutral with a reaction energy of 0.02eV but has a relatively high barrier of 1.63eV, in reasonable agreement with calculation at slightly higher coverage (E_a=1.40eV).[34] The TS is characterized by a C-O bond distance elongation from 1.18Å (I.S bond length) to 1.85Å, in which both the O and CO sit above a bridge site.

Step 41: $C + O \longrightarrow CO$. The oxygenation of carbon has a comparatively high exothermicity of -2.67eV and has an activation barrier of 1.25eV. Jorgensen and Grönbeck,[35] and Alfonso[36] both reported higher barrier for this reaction step, 1.70eV and 1.74eV, respectively, but for different functional and coverage than herein. In the TS, the C-O bond length changes from 1.19Å (I.S bond length) to 2.03Å, in which the C and O sits above a hollow and bridge site, respectively.

Step 42: $OH \longrightarrow O + H$. Dissociation of the hydroxyl molecule is slightly endothermic with a reaction energy of 0.07eV and an activation barrier of 1.06eV, in reasonable agreement with findings of Phatak et al. [32] and Scaranto and Mavrikakis[34], who calculated the activation barrier for this reaction to be 1.03eV and 1.12eV, respectively. The TS is characterized by O-H bond

elongation from 0.98Å (I.S bond length) to 1.44Å relative to the initial state, in which both O and H sit above a hollow site.

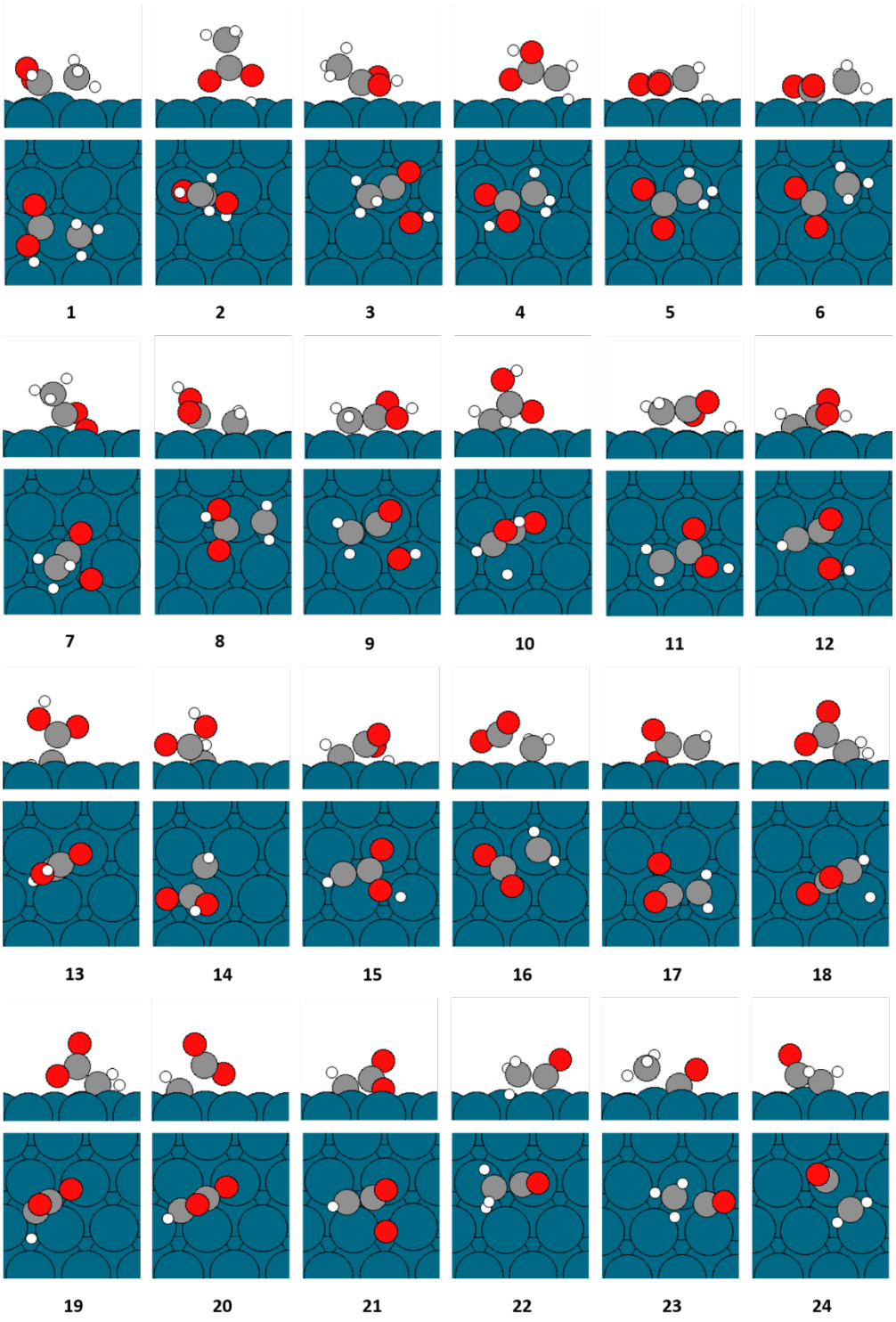

Figure 3. Side (upper panel) and top (lower panel) views of the transition states of elementary reaction 1-24 on the Pd (111) surface.

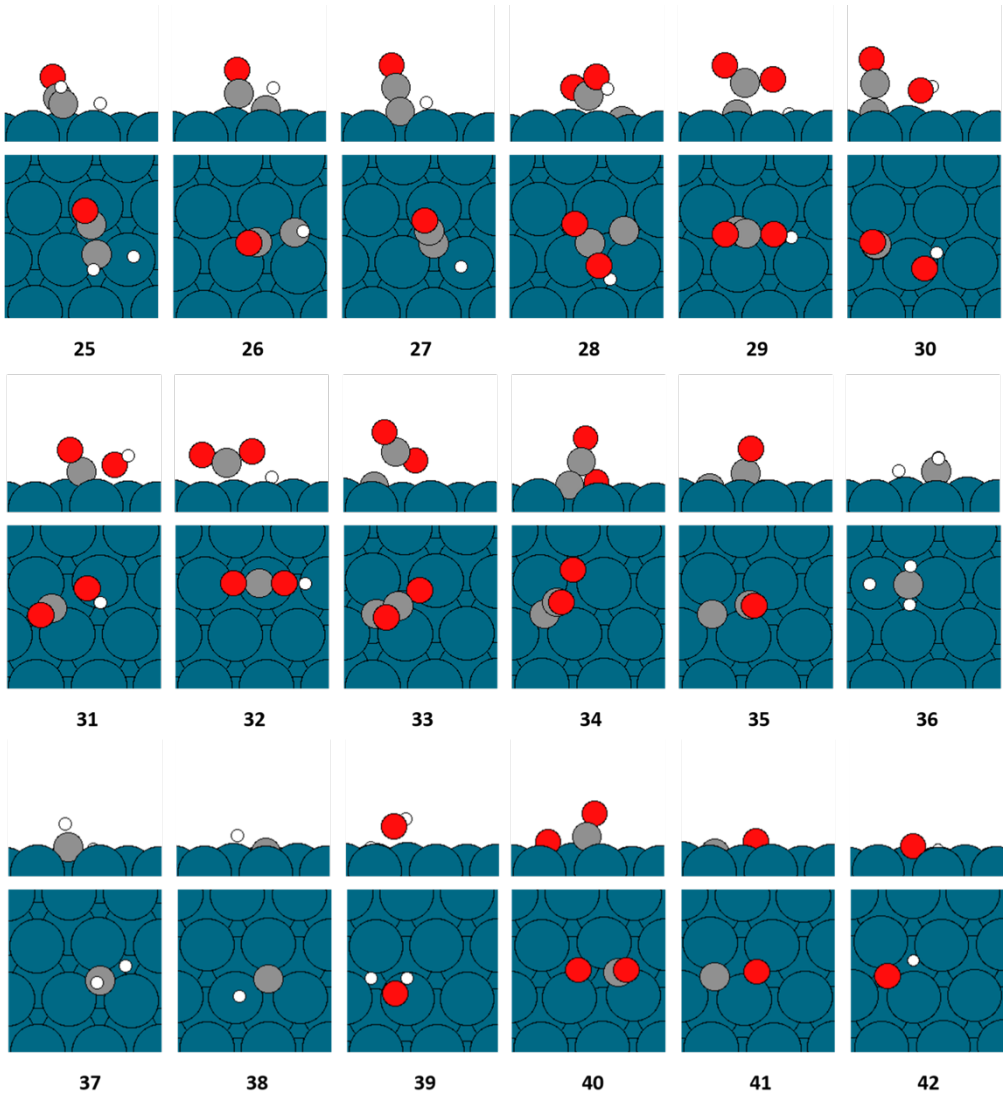

Figure 4. Side (upper panel) and top (lower panel) views of the transition states of the elementary reaction 25-42 on the Pd (111) surface.

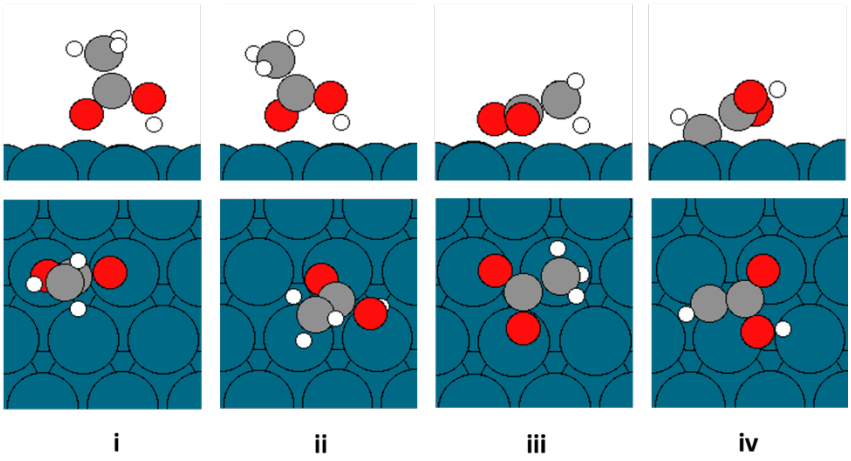

Figure 5. Snapshots of various intermediated adsorption modes used for Cl-NEB calculations and referred to in the description of the individual elementary steps 2, 3 ,6 and 15.

4. DISCUSSION

4.1 Decarboxylation (DCX) reaction pathways of acetic acid decomposition on Pd (111).

Figure 6 shows the energy diagrams of the different DCX pathways of acetic acid decomposition on Pd (111). Eleven DCX pathways were identified (see supporting information S.1 for the reaction routes of the different DCX pathways). The DCX pathways are divided into three groups depending on the initial reaction step. Four pathways starting with the dehydrogenation of the acid group (the CH_3COO-H bond) (DCX 1-4, Figure 6a), one pathway starting with C-C bond cleavage of CH_3COOH (DCX 5, Figure 6a), and six pathways starting with α-carbon dehydrogenation (the H-CH_2COOH bond) (DCX 6-11, Figure 6b).

For the DCX pathways starting with dehydrogenation of the acid group (DCX 1-4), the dehydrogenation of the CO-H bond followed by double dehydrogenations of the CH_3 group to CHCOO and finally a dissociation to CO_2 + CH, has the overall lowest activation energies (this

pathway is shown in green (DCX 3) on Figure 6a). While pathways DCX 1 and DCX 2, where CO_2 is formed directly from CH_3CO_2 and CH_2CO_2 respectively have the highest barriers. For the reaction route where the methyl group is fully dehydrogenated (DCX 4), the C-C bond cleavage has a lower activation barrier than the C-C bond cleavage for the most favorable route (DCX 3) by 0.30eV but the activation barrier of the α-carbon dehydrogenation of CHCOO to CCOO (E_a=0.79eV; DCX 4) is higher than the barrier of C-C bond scission of CHCOO to CH and CO_2 (E_a=0.61eV; DCX 3). This suggest that dehydrogenation of CHCOO to CCOO (DCX 4) is a likely less favorable pathway than DCX 3.

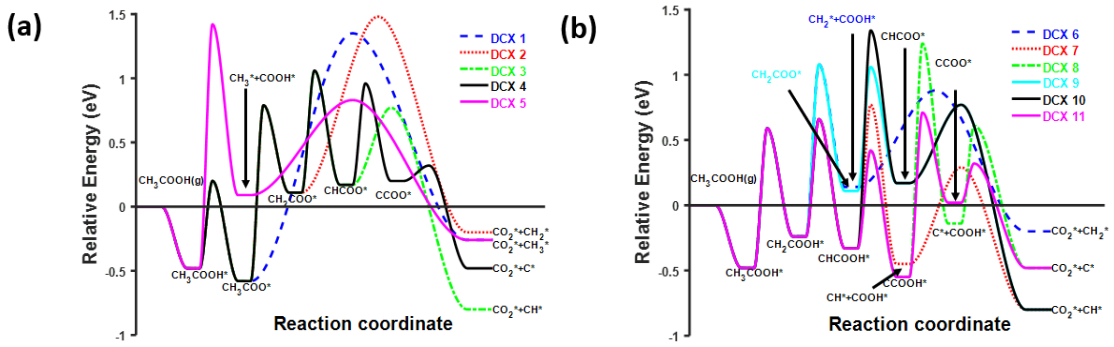

Figure 6. Energy diagrams for the DCX pathways of acetic acid decomposition on Pd (111). All values shown are with respect to gas-phase acetic acid and a clean Pd (111) slab and E_{rxn} was calculated from dissociated intermediates that are infinitely separated. Example of an energy diagram, including adsorbate-adsorbate interaction can be found in the supporting information. H* reaction products are omitted from labels for simplicity.

For reaction paths starting with dehydrogenation of the methyl group of CH_3COOH (DCX 6-11), route DCX 11, which proceeds through full dehydrogenation of the methyl group before C-C bond scission, has the lowest energy barrier height. While DCX 6, where the C-C bond scission

occurs after the initial dehydrogenation step, has a high activation barrier (E_a = 2.00eV) for the C-C bond scission, making it an unlikely pathway. Additionally, dehydrogenation of CH_2COOH to CHCOOH reduces the C-C bond cleavage barrier from 2.00eV to 1.00eV (DCX 7), but further dehydrogenation of CHCOOH to CCOOH (DCX 8) increases the activation barrier of the C-C bond cleavage from 1.00eV to 1.78eV. For both route 8 and 9, the dehydrogenation of the acid group has the highest barrier, 1.32eV for CH_2COOH to CH_2COO (DCX 9) and 1.57eV for CHCOOH to CHCOO (DCX 10), making them unlikely to be competitive reaction pathways.

In summary, DCX 3, DCX 4, DCX 7 and DCX 11 are the likely competitive reaction pathways for the DCX of acetic acid on Pd (111) of which the DCX 3 is the overall lowest energy pathway.

4.2 DCN reaction pathways of acetic acid decomposition on Pd (111).

Figure 7 and 8 show the energy diagrams of the different decarbonylation (DCN) pathways of acetic acid decomposition on Pd (111). Twenty-two DCN pathways were identified (see supporting information S.2. for the list of the different DCN pathways). Similar to the DCX pathways, the DCN pathways are divided into four groups depending on the initial reaction step. In the first six pathways (DCN 1-6, Figure 7a), the first elementary step is dehydrogenation of the CO-H bond, and the next eleven pathways (DCN 7-17, split onto two Figures 7b and 8a, for clarity), the initial elementary step is α-carbon dehydrogenation. Four pathways (DCN 18-21, Figures 8b), start with the dehydroxylation of the C-OH bond and one pathway starts with the C-C bond cleavage of CH_3COOH (DCN 22 Figures 8b).

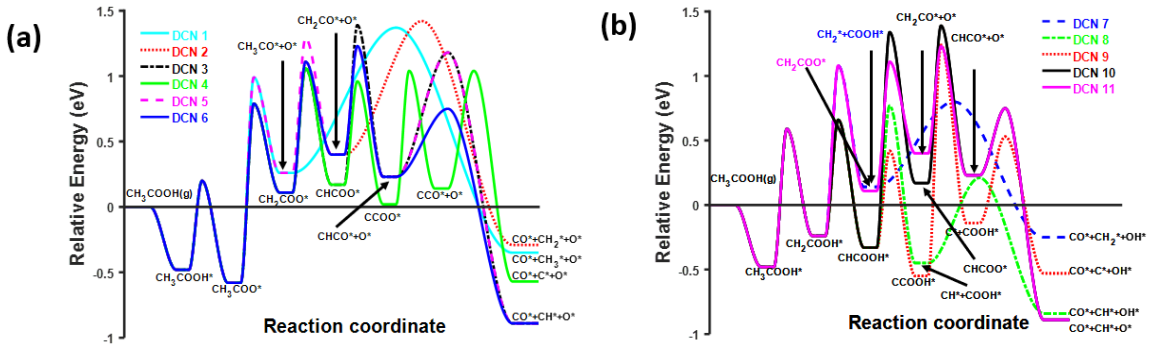

Figure 7. Energy diagrams for the DCN pathways of acetic acid decomposition on Pd (111). All energies are in respect to gas-phase acetic acid and a clean Pd (111) slab. E_{rxn} was determined from the dissociated intermediates that are infinitely separated. H* reaction products are omitted from labels for simplicity.

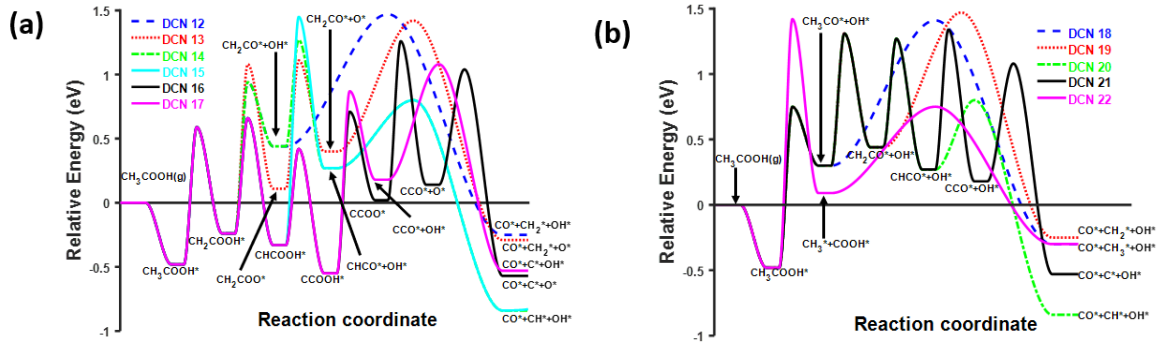

Figure 8. Energy diagram for the DCN pathways of acetic acid decomposition on Pd (111). All energies are in respect to gas-phase acetic acid and a clean Pd (111) slab. E_{rxn} was calculated for dissociated intermediates that are infinitely separated. H* reaction products are omitted from labels for simplicity.

The lowest energy DCN pathway (DCN 6) starts with dehydrogenation of the acid group, followed by α-carbon dehydrogenation, deoxygenation of the carboxylate, a second dehydrogenation of the α-carbon and finally a C-C bond scission (DCN 6: $CH_3COOH \rightarrow$

$CH_3COO+H \rightarrow CH_2COO+2H \rightarrow CH_2CO+O+2H \rightarrow CHCO+O+3H \rightarrow CH+CO+O+3H$). The highest energy step on this route is the dehydrogenation of CH_2CO to CHCO with an activation energy of 0.83eV.

Unlike the DCX pathways, further dehydrogenation of the α-carbon of CH_3CO has little effect on the C-C bond cleavage to form CO. The barrier for C-C bond cleavage decreases from 1.10eV to 1.02eV when going from CH_3CO to CH_2CO (DCN 19) but further dehydrogenation of CH_2CO to CHCO (DCN 20) substantially reduces the barrier for C-C bond cleavage from 1.02eV to 0.51eV. Same trend was previously observed for α-carbon dehydrogenation of CH_3CHCO to CH_3CCO.[31] Further dehydrogenation of CHCO to CCO (DCN 21) increases the barrier for C-C bond cleavage to 0.90eV. Additionally, the barrier for dehydrogenation of CHCO to CCO (DCN 21) is more than twice the barrier for the decarbonylation of CHCO to CH and CO (DCN 6), making DCN 21 less favorable.

The deoxygenation of CH_3COO to CH_3CO (DCN 1 and 2) has a relatively high barrier (1.56 eV) when compared to dehydrogenation of CH_3COO (E_a = 1.37eV), which makes DCN 1 and DCN 2 unlikely to occur. Dehydrogenation of CH_3COO to CH_2COO (E_a = 1.37eV) reduces the deoxygenation barrier to 0.98eV (DCN 4 and DCN 6). Unlike DCN 6, further dehydrogenation of CH_2COO to CHCOO (E_a= 0.94eV) increases deoxygenation barrier to 1.21eV (DCN 3). Dehydrogenation of CHCOO to CCOO reduces the deoxygenation barrier of CCOO to CCO (E_a =1.03eV; DCN 4) but the dehydrogenation of CHCOO (E_a =0.79eV; DCN 4) has a higher barrier than the C-C bond cleavage of CHCOO (E_a =0.61eV; DCN 6). This observation suggests that DCN 3 and DCN 4 are not one of the dominant pathways for DCN reactions due to relatively high barriers for the deoxygenation and dehydrogenation of the carboxylate.

The dehydroxylation of CH_3COOH has a relatively high activation barrier, 1.23eV, when compared to O-H bond cleavage of CH_3COOH (E_a = 0.69eV), making DCN 18-21 an unlikely competitive pathway. Following the dehydrogenation of CH_3COOH to CH_2COOH (E_a = 1.07eV), the dehydroxylation of the C-OH bond is energetically most favorable (DCN 14) with 0.14eV lower barrier than the dehydrogenation step (DCN 11 and 13). Following the initial α-carbon dehydrogenation with C-C bond cleavage ($CH_2COOH \rightarrow CH_2 + COOH$, DCN 7), has a high barrier (2.00eV), making it an unlikely favorable pathway. But further dehydrogenation (DCN 8) of CH_2COOH to CHCOOH reduces the barrier of the C-C bond cleavage to 1.00eV. Like the DCX 7 pathway, which has the same first three elementary steps as DCN 8, DCN 8 is likely a competitive pathway while DCN 9 is not a competitive pathway due to the high activation barrier of C-C bond cleavage of CCOOH (E_a = 1.78eV). After further dehydrogenation of the CH_2COOH to CHCOOH, the dehydrogenation of the acid group (DCN 10) becomes more favorable than dehydroxylation of the C-OH bond (DCN 15). Both the dehydroxylation of CHCOOH to CHCO (DCN 15) and the dehydrogenation of CHCOOH to CHCOO (DCN 10) have a comparatively high barriers,1.68eV and 1.56eV respectively, making DCN 15 and 10 an unlikely favorable pathway.

The three elementary steps following the CH_3COOH adsorption in DCN 16 and DCN 17 are α-carbon dehydrogenation to form CCOOH. The dehydrogenation of CCOOH (E_a = 1.25eV, DCN 16) has a lower barrier than the dehydroxylation (E_a = 1.42eV, DCN 17), making the DCN 16 slightly more favorable than the DCN 17 route.

In summary, DCN 6, DCN 8, DCN 14, and DCN 16 could all be competitive pathways for the DCN route with the highest overall activation barrier of 1.37eV but DCN 6 is the overall lowest energy pathway, in which the CH_3COO->CH_2COO + H elementary step has the highest barrier of 1.37eV. Figure 9 shows a Gibbs free energy diagram for the lowest energy pathways for

decarboxylation and decarbonylation (DCX 3 and DCN 6) at 300K. Routes DCX 3 and DCN 6, share the same first two elementary steps: dehydrogenations of the OH group followed by α-carbon dehydrogenation. The critical step which separates the two pathways, DCX 3 and DCN 6, are the deoxygenation of CH_2COO to CH_2CO (DCN 6) and the dehydrogenation of CH_2COO to CHCOO (DCX 3), which have free energy barriers of 0.91eV and 0.78eV, respectively, suggesting that DCX 3 is more favorable than DCN 6. Both decomposition pathways go through an acetate intermediate in good agreement with previous studies of the DCX pathway.[1, 6]

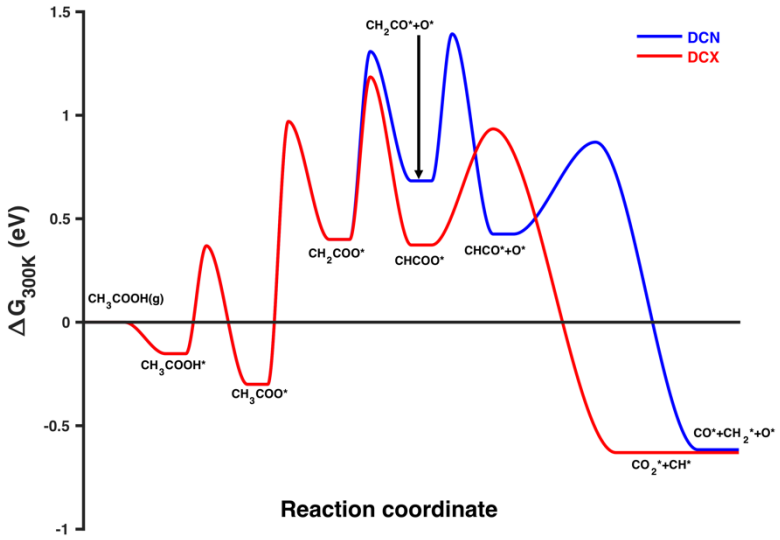

Figure 9. Gibbs free energy diagram for the most favorable DCN and DCX pathways of acetic acid decomposition on Pd (111) at 300K. All values shown are with respect to gas-phase acetic acid and a clean Pd (111) slab. H* reaction products are omitted from labels for simplicity.

4.3 Ketene as a reaction intermediate.

Experimental studies of acetic acid decomposition on Pd (111) have identified stable reaction intermediates exhibiting vibrational frequencies of 1730cm^{-1}, 1735cm^{-1}, 1745cm^{-1}, and (1230cm^{-1}-1280cm^{-1}).[4, 37-38] Augustine and Blitz[38] used DRIFTS to study Pd-catalyzed vapor phase synthesis of vinyl acetate and observed absorption bands at 1735cm^{-1} and 1230cm^{-1}-1280cm^{-1}, in which they assigned the 1735cm^{-1} band to the C-O stretching mode of a monodentate acetate (Pd ester) on Pd. Similarly, Haley et al.[4] tentatively assigned a vibrational frequency at 1735cm^{-1} to monodentate acetate in their HREELS study of acetic acid decomposition on Pd (111) in ultrahigh vacuum.

In attempt to clarify the ambiguity regarding the acetic acid intermediate which exhibit these adsorption bands on Pd (111), we compared the calculated vibrational frequency of all reaction intermediates on Pd (111) to these experimentally observed frequencies. The lowest energy reaction intermediates along the two lowest energy reaction paths is adsorbed acetate with calculated C-O stretching mode of 1617cm^{-1} and 1428cm^{-1} for mono and bidentate acetate respectively or >100cm^{-1} below the experimental frequency. Of other reaction intermediates (Table 3), only CO, CHCO and CH_2CO exhibit C-O stretching modes between 1700cm^{-1} and 1780cm^{-1}. Based on these vibrational frequency calculations, CH_2CO seems to be the strongest candidate. CH_2CO has a C-O stretching frequency of 1763cm^{-1} and a C-H stretch at 1309cm^{-1}, in reasonable agreement with 1735cm^{-1} and 1230cm^{-1}-1280cm^{-1} observed experimentally by Augustine and Blitz[38] and Haley et al,[4] but is higher in energy than the acetate intermediate. The other reaction intermediates with a C-H stretch in the 1230-1280 range are CH_2COO and CH_2, which lack the CO stretch in the 1700-1800cm^{-1} range.

This analysis does not include coverage effects or the effects of other co-adsorbates which would affect the calculated frequencies. Interestingly, a CH_2CO reaction intermediate has been suggested for acetic acid decomposition over other late transition metals (Cu and Pt).[39] Takanabe et al.[3] observed CH_2CO product on the surface in acetic acid decomposition on polycrystalline Pt and Pt/ZrO_2, and Bowker and Madix[39] observed CH_2CO in acetic acid decomposition on single-crystal Cu (110). CH_2CO has also been shown to be a precursor for C_2 oxygenates formation (ethanol and aldehydes).[40] Favre et al.[41] found that CO/H_2 on Pd/V_2O_3 starts to produce C_2 oxygenates when CH_2Cl_2 is added to the feed gas, suggesting that C_2 oxygenates formation initiates from CH_2-CO insertion to form CH_2CO on Pd/V_2O_3.

Table 3. Vibrational frequencies of mono and bidentate acetate, CH_2COO, CH_2CO, CHCO, CH_2, CH and CO on Pd (111). The frequencies are listed in units of wavenumbers, cm^{-1}. Only frequencies higher than $1200cm^{-1}$ are listed.

Adsorbed species	$\nu(CH_3)$, $\nu(CH_2)$ or $\nu(CH)$	$\nu(CO)$	$\delta(CH_3)$, $\delta(CH_2)$ or $\delta(CH)$
Bidentate acetate	3102; 3067; 3000	1428	1355; 1333
Monodentate acetate	3071; 3023	1617	
CH_2COO	3123; 3034		1297;1237
CH_2CO	3051;2972	1763	1309
CHCO	3011	1750	
CO		1776	
CH_2	3010; 2922		1279
CH	2981		
Experimental data[4, 37-38]		1730;1735;1745	1230-1280

4.4 BEP relationship for C-H, C-O and C-C bond cleavage on Pd (111).

The Brønsted-Evans-Polanyi (BEP) relationships have been used to understand trends in heterogeneous catalysis[42-47] by illustrating a linear relationship between the transition state energy and final state energy.[48-49] Figure 10 shows how the transition state energy vs the final state energy of the different C-C, C-O and C-H bond scissions follow linear trend, as expected, with slopes close to one, suggesting a late transition state.[50]

The largest deviations for C-C bond scission, estimated as the absolute value of the difference between the calculated activation energy and BEP predicted activation energy, are the C-COO and the CH-CO bond cleavages. The C-COO activation energy has an error of 0.87 eV which likely stems from the relatively low decarboxylation activation barrier (E_a = 0.31 eV). For the CH-CO bond cleavage, which has an error of 0.64eV, likely stems from the relatively large exothermic decarbonylation reaction energy (E_{rxn} = -1.04eV).

For the C-O bond scission, the CHCO-O and CCO-OH bond scissoring have the largest deviations from the BEP relationship, 0.40 eV and 0.29 eV respectively. The CHCO-O error likely originates from the comparatively low endothermic deoxygenation reaction energy (E_{rxn} = 0.35 eV), while the CCO-OH error likely originates from the large endothermic dehydroxylation reaction energy (E_{rxn} = 0.99 eV). For C-H bond scission, the largest deviation comes from the H-CH_2COOH bond scission, which has an error of 0.29eV. The H-CH_2COOH error might result from the early transition state of C-H bond cleavage of CH_3COOH but removing it from the BEP plot shifts the slope up from 0.86 to 0.94.

The BEP relationships for C-C, C-H and C-O bond scission all have a slope close to unity, indicating that the electronic structure of the transition state is like that of the final state. Additionally, a large intercept (1.36 eV) is observed for the C-C BEP relationship but a smaller intercept for the C-H (0.56 eV) and C-O (0.59 eV) BEP relationship. Combining C-H, C-O, and

C-C bond scission leads to a BEP relation of $E_{TS} = 0.88E_{FS} + 0.76$ eV (R^2=0.92) with almost 70% larger Mean Absolute Error (MAE = 0.32) for the mixed data compared to the individual BEP relations. For instance, in the mixed data, C-C bond cleavage of CHCO has the largest error of 0.82 eV, which is 0.12 eV larger than the error for C-C BEP relations. Using a BEP relations for a specific bond cleavage minimize these errors as has been proposed previously.[51]

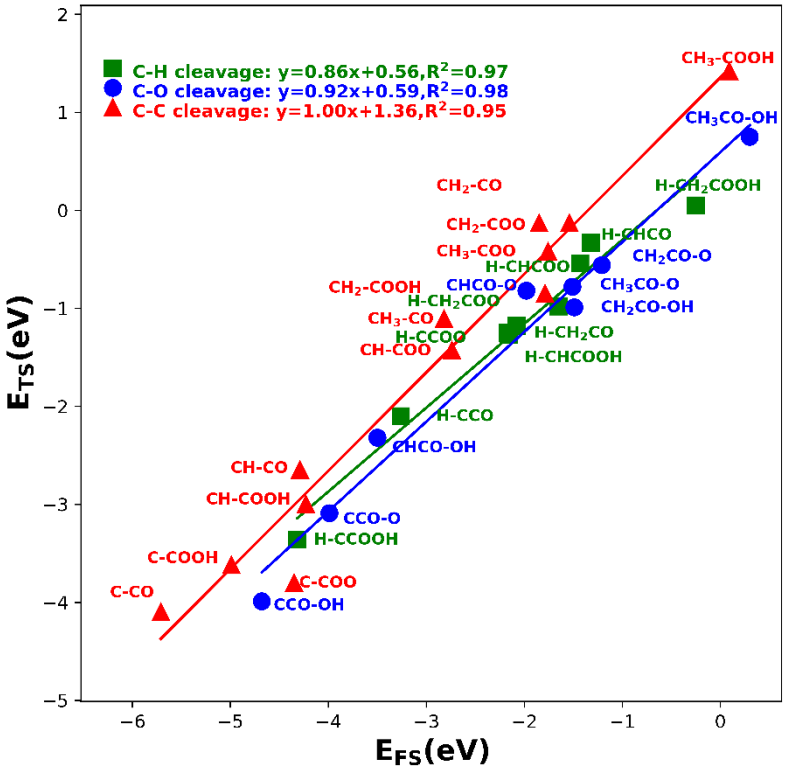

Figure 10. BEP relations for C–O cleavage (blue circle and line), C–H cleavage (green square and line), and C–C cleavage (red triangles and line) for the decarbonylation and decarboxylation of acetic acid on Pd (111). The energies of the final state (E_{FS}) and transition state (E_{TS}) are calculated relative to the energy of the corresponding reactant state in the gas phase. E_{FS} is calculated from dissociated intermediates that are infinitely separated.

5. CONCLUSIONS

We used density functional theory (DFT) to investigate the decarbonylation (DCN) and decarboxylation (DCX) mechanisms for acetic acid decomposition on Pd (111). By analyzing the minima energy pathway for 33 different reaction routes, we propose the most favorable DCN and DCX pathways.

The most energetically favorable DCN pathway proceeds via dehydrogenation of acetic acid (CH_3COOH) to acetate (CH_3COO), followed by α-carbon dehydrogenation of the acetate to carboxylmethylidene (CH_2COO) and deoxygenation of CH_2COO to ketene (CH_2CO). This is followed by dehydrogenation of CH_2CO to ketyne (CHCO) and C-C bond scission of CHCO to produce methyne (CH) and carbon monoxide (CO). The kinetically most relevant step at 300K is the dehydrogenation of the CH_2CO to CHCO.

The most favorable DCX pathway proceed via dehydrogenation of CH_3COOH to CH_3COO, followed by dehydrogenation of the CH_3COO to CH_2COO. This is followed by dehydrogenation of the CH_2COO to CHCOO and C-C bond scission of CHCOO to produce methyne (CH) and carbon dioxide (CO_2). The kinetically most relevant step is the dehydrogenation of the CH_2COO to CHCOO at 300K. The competition between DCN and DCX pathways depends on the deoxygenation of CH_2COO to CH_2CO ($G_a = 0.91$eV, DCN) and the dehydrogenation of CH_2COO to CHCOO ($G_a = 0.78$eV, DCX), in which DCX is more favorable than DCN.

This study of competitive decomposition mechanism of a small oxygenate gives insight into the overall reaction network and how by process and/or catalyst design, different reaction routes can be affected differently.

6. Corresponding Author

Email: liney.arnadottir@oregonstate.edu

7. ACKNOWLEDGEMENT

This work was supported by the National Science Foundation, CHE [Grant No. 1665287]. Part of the calculations used the Extreme Science and Engineering Discovery Environment (XSEDE) [52], through allocation TG-ENG170002 and TG-DMR160093, XSEDE is supported by National Science Foundation grant number ACI-1053575. The authors acknowledge the Texas Advanced Computing Center (TACC) at The University of Texas at Austin and the Comet cluster at the San Diego Supercomputer Center for providing HPC resources that have contributed to the research results reported within this paper. The authors thank Sean Seekins and Lynza H. Sprowl for helpful discussions.

8. SUPPORTING INFORMATION

Supporting information contains the scheme for all the DCN and DCX pathways, imaginary frequencies of all elementary reaction steps and the energy diagram of the most favorable DCN and DCX.

REFERENCES

1. Hansen, E.; Neurock, M., First-Principles Based Kinetic Simulations of Acetic Acid Temperature Programmed Reaction on Pd (111). *The Journal of Physical Chemistry B* **2001**, *105*, 9218-9229.
2. Crathorne, E.; MacGowan, D.; Morris, S.; Rawlinson, A., Application of Isotopic Transient Kinetics to Vinyl Acetate Catalysis. *Journal of Catalysis* **1994**, *149*, 254-267.
3. Takanabe, K.; Aika, K.-i.; Seshan, K.; Lefferts, L., Sustainable Hydrogen from Bio-Oil—Steam Reforming of Acetic Acid as a Model Oxygenate. *Journal of Catalysis* **2004**, *227*, 101-108.
4. Haley, R. D.; Tikhov, M. S.; Lambert, R. M., The Surface Chemistry of Acetic Acid on Pd {111}. *Catalysis letters* **2001**, *76*, 125-130.
5. Li, Z.; Gao, F.; Tysoe, W., Surface Chemistry of Acetic Acid on Clean and Oxygen-Covered Pd (1 0 0). *Surface science* **2008**, *602*, 416-423.
6. Davis, J.; Barteau, M., Hydrogen Bonding in Carboxylic Acid Adlayers on Pd (111): Evidence for Catemer Formation. *Langmuir* **1989**, *5*, 1299-1309.
7. Aas, N.; Bowker, M., Adsorption and Autocatalytic Decomposition of Acetic Acid on Pd (110). *Journal of the Chemical Society, Faraday Transactions* **1993**, *89*, 1249-1255.
8. Rachmady, W.; Vannice, M. A., Acetic Acid Hydrogenation over Supported Platinum Catalysts. *Journal of Catalysis* **2000**, *192*, 322-334.
9. Pallassana, V.; Neurock, M., Reaction Paths in the Hydrogenolysis of Acetic Acid to Ethanol over Pd(111), Re(0001), and Pdre Alloys. *Journal of Catalysis* **2002**, *209*, 289-305.
10. Wang, Z.; Li, G.; Liu, X.; Huang, Y.; Wang, A.; Chu, W.; Wang, X.; Li, N., Aqueous Phase Hydrogenation of Acetic Acid to Ethanol over Ir-Moo X/Sio 2 Catalyst. *Catalysis Communications* **2014**, *43*, 38-41.

11. Olcay, H.; Xu, L.; Xu, Y.; Huber, G. W., Aqueous-Phase Hydrogenation of Acetic Acid over Transition Metal Catalysts. *ChemCatChem* **2010**, *2*, 1420-1424.
12. Zhang, S.; Duan, X.; Ye, L.; Lin, H.; Xie, Z.; Yuan, Y., Production of Ethanol by Gas Phase Hydrogenation of Acetic Acid over Carbon Nanotube-Supported Pt–Sn Nanoparticles. *Catalysis today* **2013**, *215*, 260-266.
13. Rachmady, W.; Vannice, M. A., Acetic Acid Reduction by H_2 over Supported Pt Catalysts: A Drifts and Tpd/Tpr Study. *Journal of Catalysis* **2002**, *207*, 317-330.
14. Carnahan, J.; Ford, T.; Gresham, W.; Grigsby, W.; Hager, G., Ruthenium-Catalyzed Hydrogenation of Acids to Alcohols. *Journal of the American Chemical Society* **1955**, *77*, 3766-3768.
15. Li, M.; Guo, W.; Jiang, R.; Zhao, L.; Shan, H., Decomposition of Ethanol on Pd (111): A Density Functional Theory Study. *Langmuir* **2009**, *26*, 1879-1888.
16. Kresse, G.; Hafner, J., Ab Initio Molecular Dynamics for Liquid Metals. *Physical Review B* **1993**, *47*, 558.
17. Kresse, G.; Hafner, J., Ab Initio Molecular-Dynamics Simulation of the Liquid-Metal–Amorphous-Semiconductor Transition in Germanium. *Physical Review B* **1994**, *49*, 14251.
18. Kresse, G.; Furthmüller, J., Efficiency of Ab-Initio Total Energy Calculations for Metals and Semiconductors Using a Plane-Wave Basis Set. *Computational materials science* **1996**, *6*, 15-50.
19. Kresse, G.; Furthmüller, J., Efficient Iterative Schemes for Ab Initio Total-Energy Calculations Using a Plane-Wave Basis Set. *Physical review B* **1996**, *54*, 11169.
20. Blöchl, P. E., Projector Augmented-Wave Method. *Physical review B* **1994**, *50*, 17953.
21. Perdew, J. P.; Yue, W., Accurate and Simple Density Functional for the Electronic Exchange Energy: Generalized Gradient Approximation. *Physical review B* **1986**, *33*, 8800.
22. Perdew, J. P.; Chevary, J. A.; Vosko, S. H.; Jackson, K. A.; Pederson, M. R.; Singh, D. J.; Fiolhais, C., Atoms, Molecules, Solids, and Surfaces: Applications of the Generalized Gradient Approximation for Exchange and Correlation. *Physical Review B* **1992**, *46*, 6671.
23. White, J.; Bird, D., Implementation of Gradient-Corrected Exchange-Correlation Potentials in Car-Parrinello Total-Energy Calculations. *Physical Review B* **1994**, *50*, 4954.
24. Ashcroft, N. W.; Mermin, N. D., Solid State Physics., Holt, Rinehart and Winston., **1976**, Pp 70.
25. Henkelman, G.; Uberuaga, B. P.; Jónsson, H., A Climbing Image Nudged Elastic Band Method for Finding Saddle Points and Minimum Energy Paths. *The Journal of chemical physics* **2000**, *113*, 9901-9904.
26. Henkelman, G.; Jónsson, H., Improved Tangent Estimate in the Nudged Elastic Band Method for Finding Minimum Energy Paths and Saddle Points. *The Journal of chemical physics* **2000**, *113*, 9978-9985.
27. Sheppard, D.; Terrell, R.; Henkelman, G., Optimization Methods for Finding Minimum Energy Paths. *The Journal of chemical physics* **2008**, *128*, 134106.
28. Jónsson, H.; Mills, G.; Jacobsen, K. W., Nudged Elastic Band Method for Finding Minimum Energy Paths of Transitions. In *Classical and Quantum Dynamics in Condensed Phase Simulations*, World Scientific: 1998; pp 385-404.
29. Hensley, A. J.; Wang, Y.; Mei, D.; McEwen, J.-S., Mechanistic Effects of Water on the Fe-Catalyzed Hydrodeoxygenation of Phenol. The Role of Brønsted Acid Sites. *ACS Catalysis* **2018**, *8*, 2200-2208.
30. James, J.; Saldin, D. K.; Zheng, T.; Tysoe, W. T.; Sholl, D. S., Structure and Binding Site of Acetate on Pd(111) Determined Using Density Functional Theory and Low Energy Electron Diffraction. *Catalysis Today* **2005**, *105*, 74-77.
31. Lu, J.; Behtash, S.; Heyden, A., Theoretical Investigation of the Reaction Mechanism of the Decarboxylation and Decarbonylation of Propanoic Acid on Pd (111) Model Surfaces. *The Journal of Physical Chemistry C* **2012**, *116*, 14328-14341.
32. Phatak, A. A.; Delgass, W. N.; Ribeiro, F. H.; Schneider, W. F., Density Functional Theory Comparison of Water Dissociation Steps on Cu, Au, Ni, Pd, and Pt. *The Journal of Physical Chemistry C* **2009**, *113*, 7269-7276.

33. Grabow, L. C.; Gokhale, A. A.; Evans, S. T.; Dumesic, J. A.; Mavrikakis, M., Mechanism of the Water Gas Shift Reaction on Pt: First Principles, Experiments, and Microkinetic Modeling. *The Journal of Physical Chemistry C* **2008**, *112*, 4608-4617.
34. Scaranto, J.; Mavrikakis, M., Density Functional Theory Studies of HCOOH Decomposition on Pd (111). *Surface Science* **2016**, *650*, 111-120.
35. Jørgensen, M.; Grönbeck, H., First-Principles Microkinetic Modeling of Methane Oxidation over Pd (100) and Pd (111). *ACS Catalysis* **2016**, *6*, 6730-6738.
36. Alfonso, D. R., Comparative Studies of CO and H_2O Interactions with Pd (111) Surface: A Theoretical Study of Poisoning. *Applied physics letters* **2006**, *88*, 051908.
37. Macleod, N.; Keel, J. M.; Lambert, R. M., The Effects of Ageing a Bimetallic Catalyst under Industrial Conditions: A Study of Fresh and Used Pd-Au-K/Silica Vinyl Acetate Synthesis Catalysts. *Applied Catalysis A: General* **2004**, *261*, 37-46.
38. Augustine, S. M.; Blitz, J. P., The Use of Drifts-Ms and Kinetic Studies to Determine the Role of Acetic Acid in the Palladium-Catalyzed Vapor-Phase Synthesis of Vinyl Acetate. *Journal of Catalysis* **1993**, *142*, 312-324.
39. Bowker, M.; Madix, R. J., The Adsorption and Oxidation of Acetic Acid and Acetaldehyde on Cu (110). *Applications of Surface Science* **1981**, *8*, 299-317.
40. Lee, G. d.; Ponec, V., On Some Problems of Selectivity in Syngas Reactions on the Group Viii Metals. *Catalysis Reviews Science and Engineering* **1987**, *29*, 183-218.
41. Favre, T. L. F.; van der Lee, G.; Ponec, V., Heterogeneous Catalytic Insertion Mechanism of the C_2 Oxygenate Formation. *Journal of the Chemical Society, Chemical Communications* **1985**, 230-231.
42. Nørskov, J. K.; Bligaard, T.; Hvolbæk, B.; Abild-Pedersen, F.; Chorkendorff, I.; Christensen, C. H., The Nature of the Active Site in Heterogeneous Metal Catalysis. *Chemical Society Reviews* **2008**, *37*, 2163-2171.
43. Nørskov, J. K.; Bligaard, T.; Logadottir, A.; Bahn, S.; Hansen, L. B.; Bollinger, M.; Bengaard, H.; Hammer, B.; Sljivancanin, Z.; Mavrikakis, M., Universality in Heterogeneous Catalysis. *Journal of Catalysis* **2002**, *209*, 275-278.
44. Michaelides, A.; Liu, Z.-P.; Zhang, C.; Alavi, A.; King, D. A.; Hu, P., Identification of General Linear Relationships between Activation Energies and Enthalpy Changes for Dissociation Reactions at Surfaces. *Journal of the American Chemical Society* **2003**, *125*, 3704-3705.
45. Bligaard, T.; Nørskov, J. K.; Dahl, S.; Matthiesen, J.; Christensen, C. H.; Sehested, J., The Brønsted–Evans–Polanyi Relation and the Volcano Curve in Heterogeneous Catalysis. *Journal of Catalysis* **2004**, *224*, 206-217.
46. Alcala, R.; Mavrikakis, M.; Dumesic, J. A., DFT Studies for Cleavage of C-C and C-O Bonds in Surface Species Derived from Ethanol on Pt (111). *Journal of Catalysis* **2003**, *218*, 178-190.
47. Liu, B.; Greeley, J., Decomposition Pathways of Glycerol Via C–H, O–H, and C–C Bond Scission on Pt (111): A Density Functional Theory Study. *The Journal of Physical Chemistry C* **2011**, *115*, 19702-19709.
48. Bronsted, J., Acid and Basic Catalysis. *Chemical Reviews* **1928**, *5*, 231-338.
49. Evans, M.; Polanyi, M., Inertia and Driving Force of Chemical Reactions. *Transactions of the Faraday Society* **1938**, *34*, 11-24.
50. Jens, K.; Studt, F.; Abild-Pedersen, F.; Bligaard, T., *Fundamental Concepts in Heterogeneous Catalysis*; John Wiley & Sons, 2014.
51. Wang, S.; Temel, B.; Shen, J.; Jones, G.; Grabow, L. C.; Studt, F.; Bligaard, T.; Abild-Pedersen, F.; Christensen, C. H.; Nørskov, J. K., Universal Brønsted-Evans-Polanyi Relations for C–C, C–O, C–N, N–O, N–N, and O–O Dissociation Reactions. *Catalysis letters* **2011**, *141*, 370-373.
52. Towns, J.; Cockerill, T.; Dahan, M.; Foster, I.; Gaither, K.; Grimshaw, A.; Hazlewood, V.; Lathrop, S.; Lifka, D.; Peterson, G. D., et al., Xsede: Accelerating Scientific Discovery. *Computing in Science & Engineering* **2014**, *16*, 62-74.

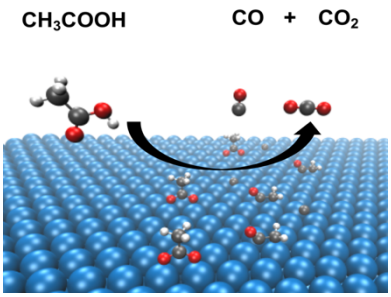

TOC Graphics